Jackson, T.R., Salmina, K., Huna, A., Inashkina, I., Jankevics, E., Riekstina, U., Kalnina, Z., Ivanov, A., Townsend, P.A., Cragg, M.S., and Erenpreisa, J. (2013) DNA damage causes TP53-dependent coupling of self-renewal and senescence pathways in embryonal carcinoma cells. Cell Cycle, 12 (3). pp. 430-441. ISSN 1538-4101

Copyright © 2013 Landes Bioscience

http://eprints.gla.ac.uk/74546/

Deposited on: 05 February 2013

Enlighten – Research publications by members of the University of Glasgow
http://eprints.gla.ac.uk

Landes Bioscience www.landesbioscience.com

Supplemental Material to:

Thomas R. Jackson, Kristine Salmina, Anda Huna, Inna Inashkina, Eriks Jankevics, Una Riekstina, Zane Kalnina, Andrey Ivanov, Paul A. Townsend, Mark S. Cragg and Jekaterina Erenpreisa

DNA damage causes TP53-dependent coupling of self-renewal and senescence pathways in embryonal carcinoma cells

Cell Cycle 2012; 12(3)
http://dx.doi.org/10.4161/cc.23285

http://www.landesbioscience.com/journals/cc/article/23285

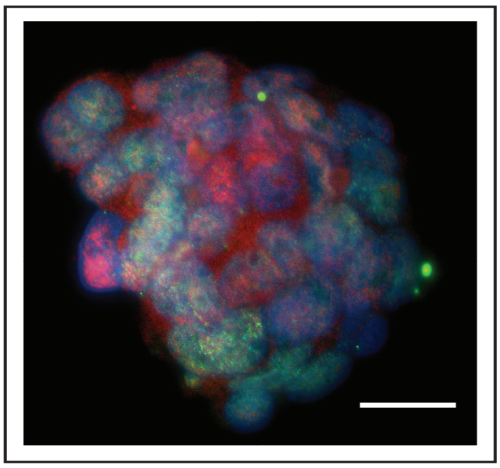

SF1. PA1 cells seeded into serum free media readily form non-adherent. OCT4/NANOG-positive spheric cell aggregates, indicating to the pluripotent (ES) cell properties of this cell line. Cells were stained for NANOG (green), OCT4AB (red) and counter stained with DAPI (Blue). Bar = 20 µm. Representative images from 2 independent experiments.

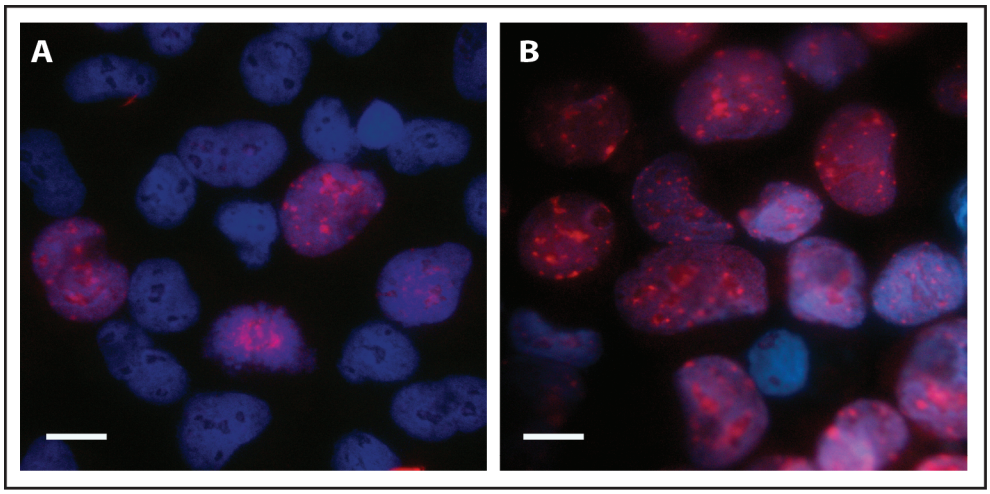

SF2. Up-regulation of AURORA B kinase in response to ETO treatment assessed by IF in combination with DAPI (blue). (A) In non-treated PA1 cells AURORA B kinase (red) labels centromeres of metaphase chromosomes and G2 cell nuclei; (B) In ETO- treated PA1 cells the enhanced AURORA B kinase staining is apparent in the majority of interphase cells arrested on day 2 in G2. This enhanced staining subsequently persists in most cells with large nuclei indicating to their mitotic potential. Bars = 10µm. Representative images from 6 independent experiments.

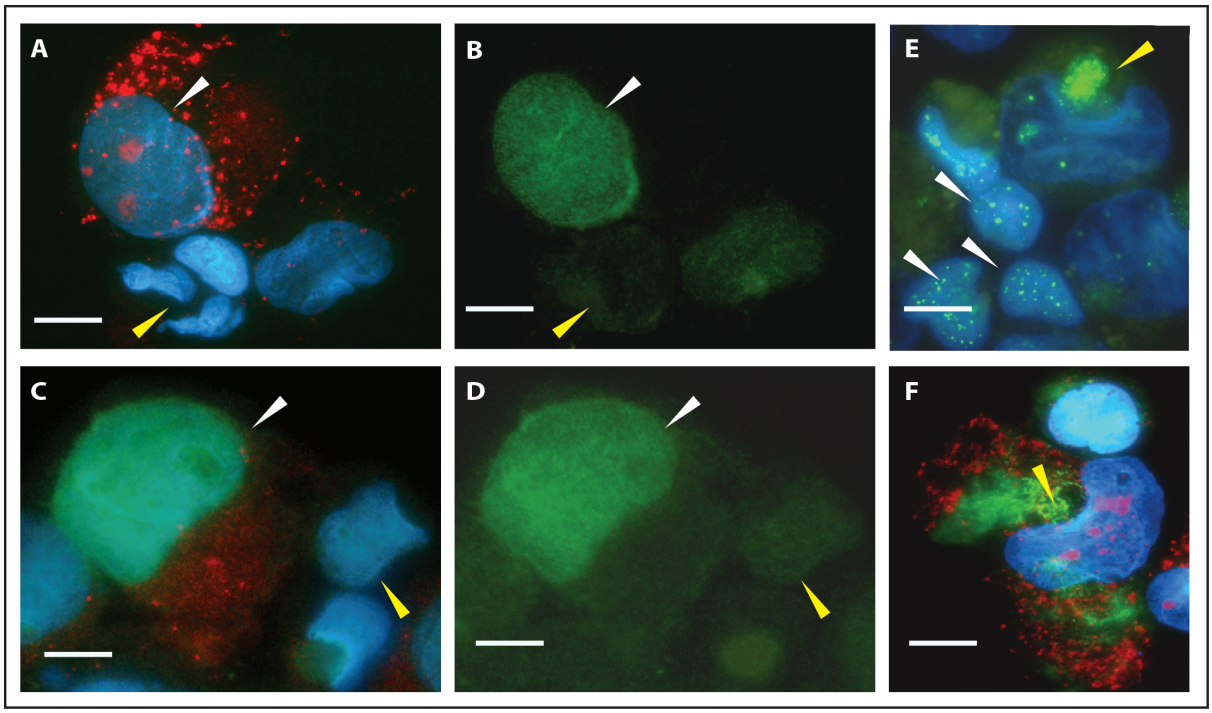

SF3. Characteristics of macroautophagy and expression of OCT4A and telomerase (TERT) in different cell populations on day 5 post ETO treatment. PA-1 cells were treated with 8μM ETO for 20 hours, then washed and examined 5 days later. Fixed cells were stained for LC3B (red; panel A and F), OCT4A (green; panel B, C and D), P62 (red; panel C) or TERT (green; panel E and F) in combination with DAPI (blue). (A-D) Macroautophagy marked by LC3B and P62 is characteristic of large hypertrophic cells, possessing extensive OCT4A (white arrowheads) and not small diploid cells with relatively low OCT4A levels (yellow arrowheads) which are recovering and re-entering the mitotic cycle. These small diploid cell nuclei possess nuclear TERT foci (white arrowheads on E), testifying to their self-renewal potential. (E, F) Hypertrophic (presumably pre-senescent) cells undergoing enhanced macroautophagy release the chromatin-bound TERT in perinuclear autophagic vacuoles (yellow arrowheads), whilst accumulating large amounts of TERT in the cytosol. Both phenomena are indicative of an apoptosis-protective function, which may be supported by OCT4. Bars = 10μm. Representative images from 3 independent experiments.

A)

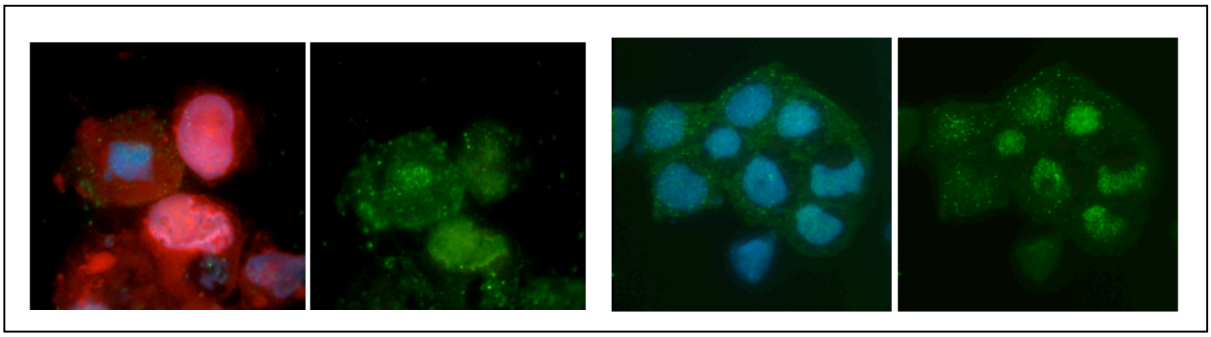

B)

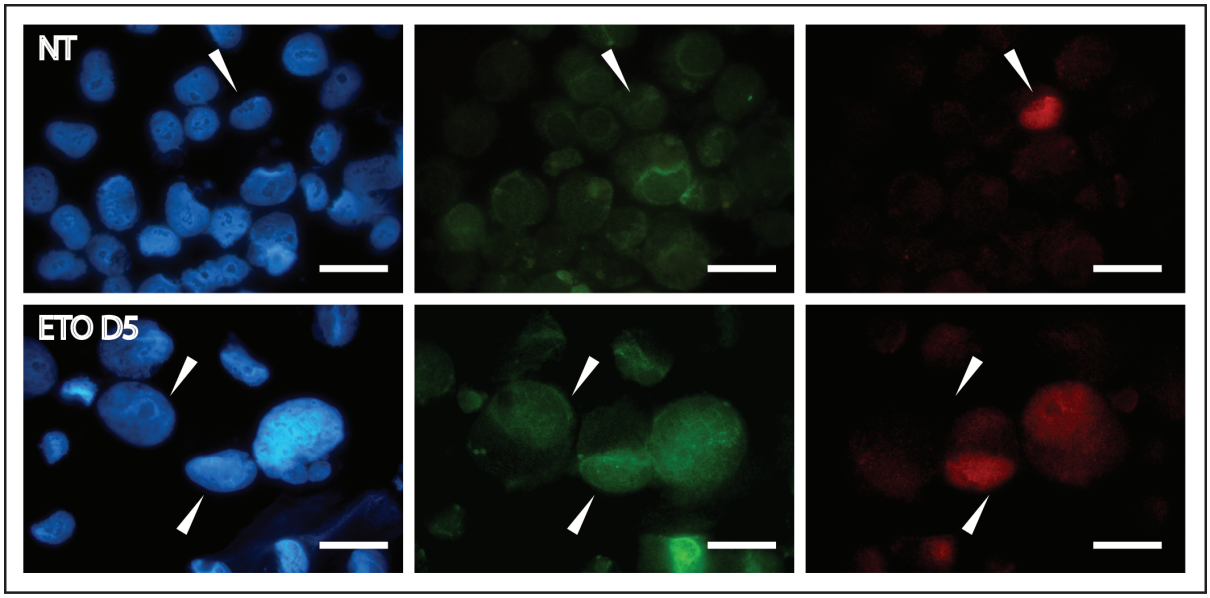

SF4. NANOG expression in PA-1 cells. PA-1 cells were treated with 8μM ETO for 20 hours, then washed and examined by IF for A) OCT4A (red) or NANOG (green) and DAPI (blue) at day 5 or B) OCT4A (green) or NANOG (red) and DAPI (blue). A) NANOG outlines chromosomes in the mitoses and small clones of recovering cells. B) Rare NT cells display high levels of NANOG expression (white arrowheads). Large, presumably polyploid cells also have high levels of NANOG expression (white arrowheads). Bar = 10μm. Representative data from 7 independent experiments using either monoclonal or polyclonal anti-NANOG antibody.

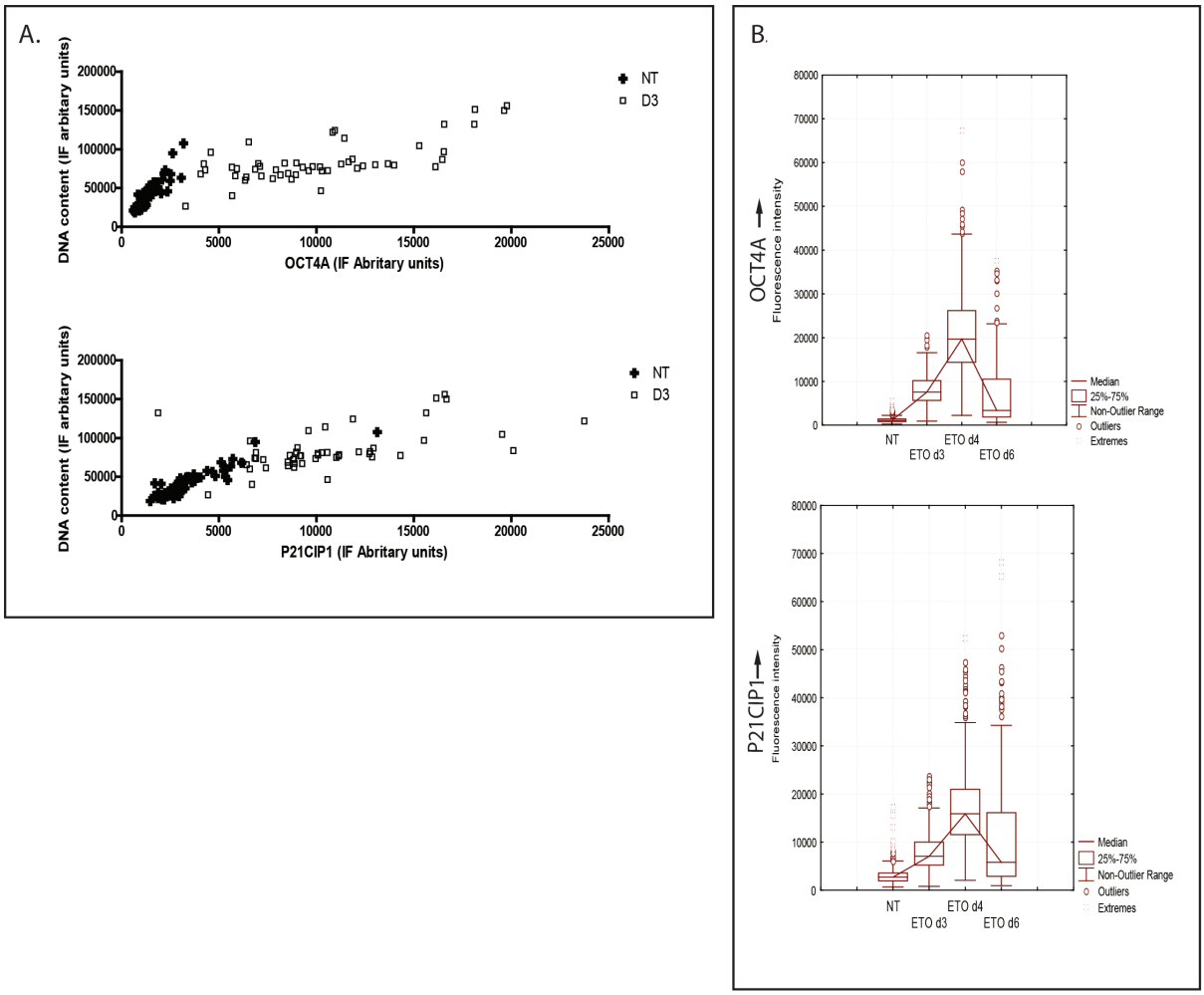

SF5. Expression levels of OCT4A and P21CIP1 in PA-1 cells in response to ETO treatment as determined using image cytometry. PA-1 cells were treated with 8μM ETO for 20 hours, then washed and analysed over time for OCT4A or P21CIP1 expression in combination with DAPI. (A) The fluorescent intensity of P21CIP1 and OCT4A staining was determined by image cytometry and plotted against the DNA content for 50 cells. OCT4A (top) and P21CIP1 (bottom) have higher levels of expression in cells with ≥4C DNA content after ETO treatment. (B) Shows the median, inter quartile range, full range and outliers of the OCT4A (top) and P21CIP1 (bottom) intensities on day 3, 4 and 6 after ETO treatment compared to NT controls (500 cells). Greatly increased heterogeneity in OCT4A and P21CIP1 content is evident after ETO treatment, with mean expression peaking on day 4. Data are representative of >3 independent experiments.

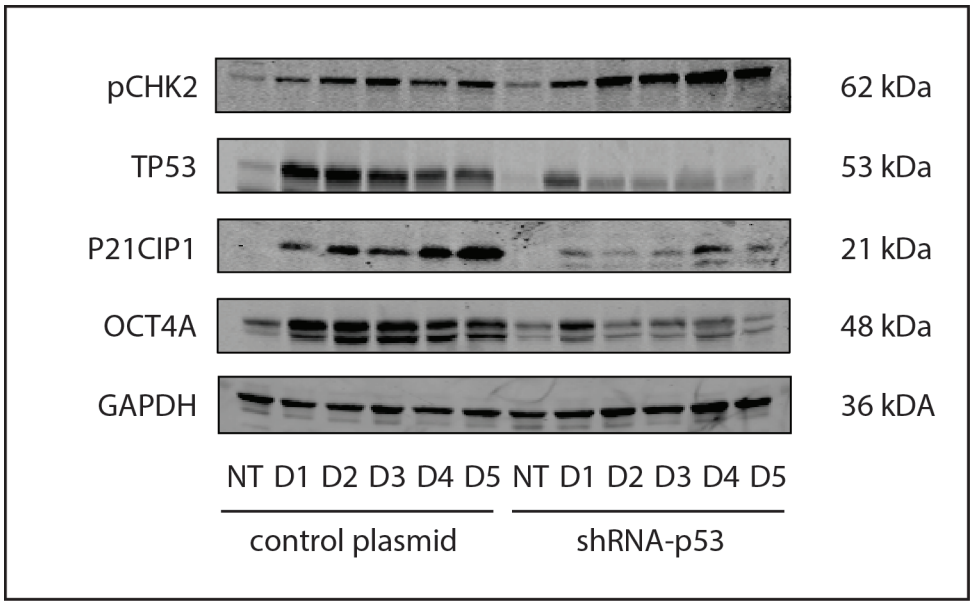

SF6. Immunoblot analysis of TP53, pCHK2, OCT4A and P21CIP1 in PA-1 cells after ETO treatment. PA-1 cells were stably transfected with shRNA-P53 or control vector before treatment with 8μM ETO, washing after 20 hours, cell lysates generated and assessed by immunoblotting for pCHK2, TP53, P21CIP1, OCT4A or GAPDH as a loading control at the indicated time points. TP53 was up regulated in response to ETO treatment and suppressed by shRNA-TP53. P21CIP1 and OCT4A were also up-regulated by ETO treatment and the upregulation was restricted by silencing of TP53. pCHK2 accumulated in ETO treated cells and this accumulation was increased in TP53 silenced cells. Data are representative of 3 independent experiments.

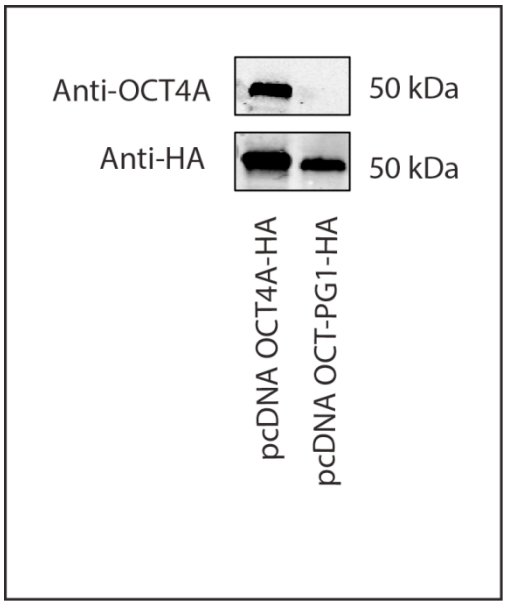

SF7. Immunoblot analysis of HA tagged OCT4A and OCT4-PG1 isoforms expressed in HEK 293T cells. 293T cells were transiently transfected with plasmids encoding HA tagged OCT4A and OCT4-PG1 isoforms. 24 hours later, cell lysates were made and immunoblotting performed for OCT4A or HA as a loading control. These data clearly show that the OCT4A antibody detects OCT4A but not OCT4-PG1. Data shown from a single experiment.

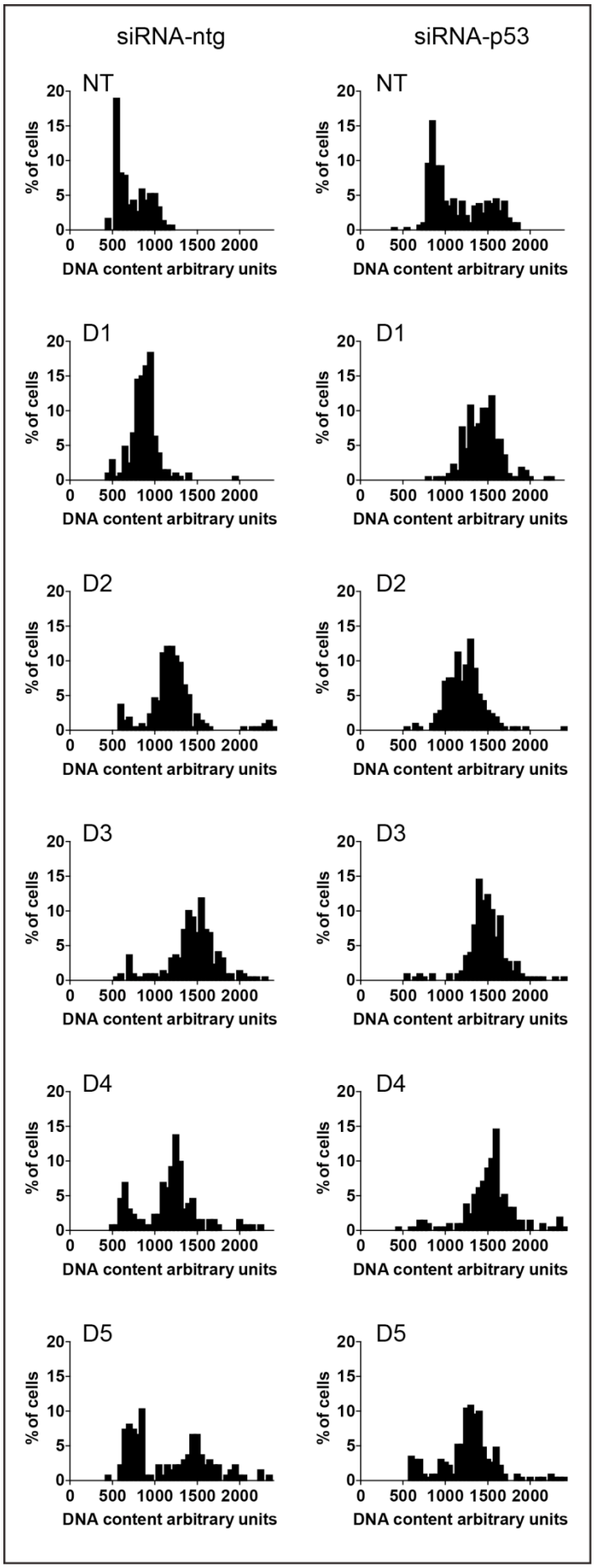
siRNA-ntg
siRNA-p53
NT
NT
D1
D1
D2
D2
D3
D3
D4
D4
D5
D5
% of cells
0
5
10
15
20
0
500
1000
1500
2000
DNA content arbitrary units

SF8. Effect of TP53-silencing on the dynamics of the cell cycle response to ETO in PA-1 cells. PA-1 cells transfected with siRNA-p53 or ntg control were treated with 8μM ETO for 20 hours, then washed and examined by DNA image cytometry over time. siRNA-TP53 caused a larger accumulation of cells in the 4C fraction (which may be composed of (2N-G2, M, and 4N-G1 cells) and delayed recovery of the proliferatiing G1-2C fraction as compared with the ntg control ETO-treated cells on days 4 and 5. Representative histograms from two independent experiments.

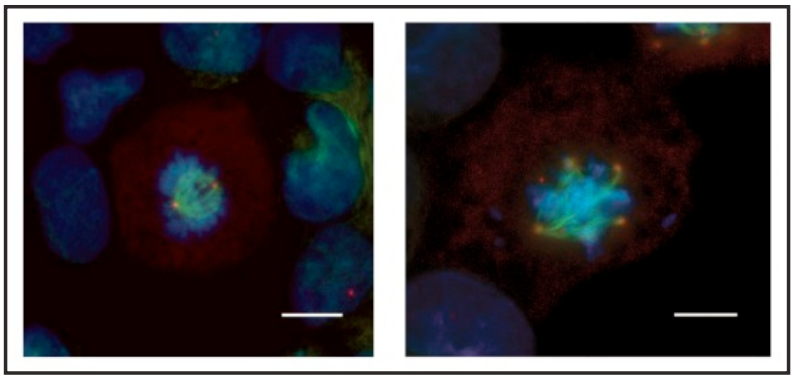

SF9. Examples of normal and abnormal mitoses. Cells were pelleted, cytospun, fixed and stained for pCHK2 (red) and α-tubulin (green) to allow analyses of centrosomes and spindles. The left panel shows normal bi-centrosomal/bi-polar mitosis in NT cells; the right panel shows multicentrosomal/multipolar dysregulated mitosis in ETO treated cells. Bar = 10μM. Representative images from 3 independent experiments.

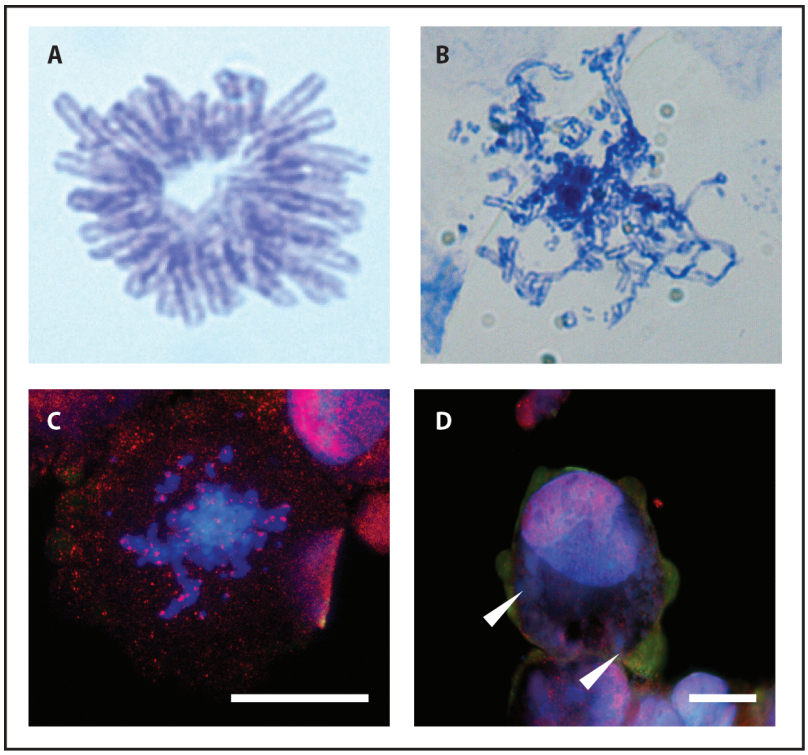

SF10. Examples of normal and aberrant mitoses in PA-1 cells before or after ETO treatment. PA-1 cells (A) or siRNAp53 treated cells (B-D) were untreated or treated with 8μM ETO for 20 hours, then washed and assessed by IF or stained with toluidine blue on day 4. For IF, fixed cytospins were stained for γH2AX (red; panel C and D), in combination with DAPI (blue). For DNA imaging cells were treated with 5N HCl and stained with toluidine blue.(A) normal metaphase plate; (B) highly aberrant mitosis stained for DNA after siRNA-p53 treatment; (C) aberrant mitosis with many chromosomes unattached to the spindle and possessing DNA damage as judged by γH2AX staining. (D) A cell with persistent DNA damage undergoing mitotic slippage, while the re-formation of the nuclear envelope leaves behind multiple micronuclei in the cytoplasm (arrowheads); Bar = 10 μm. Representative images from 4 independent experiments.